






Article

Impact Assessment of Dynamic Loading Induced by the Provision of Frequency Containment Reserve on the Main Bearing Lifetime of a Wind Turbine

Narender Singh ^{1,2,*} , Dibakor Boruah ¹ , Jeroen D. M. De Kooning ^{1,2} , Wim De Waele ¹  and Lieven Vandeveld ^{1,2} 

¹ Department of Electromechanical, Systems & Metal Engineering, Faculty of Engineering & Architecture, Ghent University, Tech Lane Ghent Science Park—Campus A, Technologiepark-Zwijnaarde 131, B-9052 Ghent, Belgium

² FlandersMake@UGent—Corelab MIRO, Flanders Make, B-9052 Ghent, Belgium

* Correspondence: narender.singh@ugent.be

Abstract: The components of an operational wind turbine are continuously impacted by both static and dynamic loads. Regular inspections and maintenance are required to keep these components healthy. The main bearing of a wind turbine is one such component that experiences heavy loading forces during operation. These forces depend on various parameters such as wind speed, operating regime and control actions. When a wind turbine provides frequency containment reserve (FCR) to support the grid frequency, the forces acting upon the main bearing are also expected to exhibit more dynamic variations. These forces have a direct impact on the lifetime of the main bearing. With an increasing trend of wind turbines participating in the frequency ancillary services market, an analysis of these dynamic forces becomes necessary. To this end, this paper assesses the effect of FCR-based control on the main bearing lifetime of the wind turbine. Firstly, a control algorithm is implemented such that the output power of the wind turbine is regulated as a function of grid frequency and the amount of FCR. Simulations are performed for a range of FCR to study the changing behaviour of dynamical forces acting on the main bearing with respect to the amount of FCR provided. Then, based on the outputs from these simulations and using 2 years of LiDAR wind data, the lifetime of the main bearing of the wind turbine is calculated and compared for each of the cases. Finally, based on the results obtained from this study, the impact of FCR provision on the main bearing lifetime is quantified and recommendations are made, that could be taken into account in the operation strategy of a wind farm.

Keywords: frequency containment reserve; structural loading; wind energy; wind turbine control; wind turbine main bearing



Citation: Singh, N.; Boruah, D.; De Kooning, J.D.M.; De Waele, W.; Vandeveld, L. Impact Assessment of Dynamic Loading Induced by the Provision of Frequency Containment Reserve on the Main Bearing Lifetime of a Wind Turbine. *Energies* **2023**, *16*, 2851. <https://doi.org/10.3390/en16062851>

Academic Editors: Galih Bangga and Martin Otto Laver Hansen

Received: 21 February 2023

Revised: 16 March 2023

Accepted: 16 March 2023

Published: 19 March 2023



Copyright: © 2023 by the authors. Licensee MDPI, Basel, Switzerland. This article is an open access article distributed under the terms and conditions of the Creative Commons Attribution (CC BY) license (<https://creativecommons.org/licenses/by/4.0/>).

1. Introduction

The wind power sector has shown a remarkable growth in the past decade with no foreseeable sign of diminishing. Figure 1 presents the globally installed wind energy capacity from 2012 to 2021. In 2021, nearly 94 GW of new wind power was installed globally, including 22.1 GW of offshore wind capacity. At the end of 2021 the total global wind power capacity reached 824 GW. It is expected that by 2026 the global installed wind capacity will reach 1394 GW [1,2]. With the targets of the European Union (EU) to reduce greenhouse gas emissions, a trend of increasing renewable energy penetration in the power systems has been observed [3]. In 2021, Europe added 17 GW of new wind power capacity. This adds up to a total of 236 GW of installed wind energy capacity in Europe. In 2021, 15% of the total electricity consumed by all EU-nations was generated by using wind energy [4].

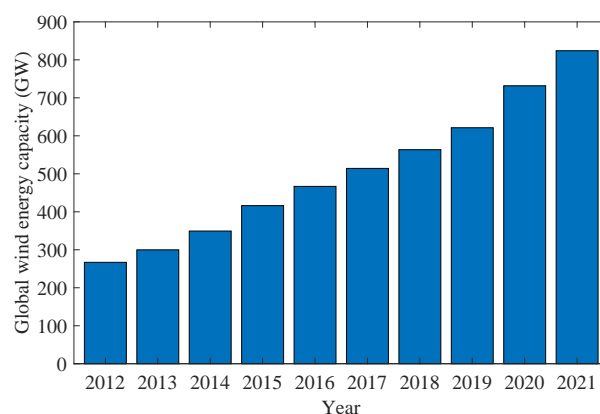


Figure 1. Global wind energy installed capacity.

With the increasing share of wind energy, an active participation of the wind farms in the ancillary services market is expected, and even obliged by the grid code in some countries [5]. Some ancillary services such as frequency containment reserve (FCR), fast frequency response (FFR), synchronous inertial response (SIR), enhanced frequency response (EFR) and fast post-fault active power recovery (FPFAPR), provide opportunities for wind farms to participate in the ancillary services market [6].

Along with the increasing share of wind energy in the energy mix and an increased participation of wind farms in ancillary service markets, there is a growing concern about the structural health and maintenance of wind turbine components. As a wind turbine or wind farm ages, the overall performance is reduced. The age-based performance of a wind farm was investigated in [7]. A survey of failures of Swedish wind farms is presented in [8]. Reliability analysis and probabilistic methods for wind farm performance are presented in [9,10]. Methods to quantify the availability of wind farms were proposed in [11]. An extensive data study presented in [12] found that wind turbines lose around 1.6% of their nominal output per year due to aging. It has also been seen that some wind turbine components fail before their expected lifetime [13]. To fill this gap, several studies have been conducted that explore new methods of wind turbine monitoring and maintenance. A deep learning approach was explored to predict the remaining useful life of rotating components in [14]. A cost-effective condition monitoring for wind turbines was proposed in [15]. Different methods of wind turbine maintenance management were suggested in [16,17]. The approach for a remote condition monitoring system was explored in [18]. Wind turbine failure detection and condition-based maintenance strategies are presented in [19] and [20], respectively. In terms of the overall optimization of a wind farm, a study exploring wind farm layout optimization is presented in [21].

These studies are focused on overall wind farms or single turbines as a whole. However, specific studies based on important individual wind turbine components are rare. A crucial component of the wind turbine is its main bearing. A downtime due to a main bearing failure can cause a significant loss of revenue in addition to high replacement costs. There are several factors that affect the health of a bearing. Foremost, the manufacturing quality of the bearing is critical to a long service life. Logistics of storage, application and mounting also play an important role. Furthermore, it is crucial for the bearing to be well lubricated. The lubrication specifications and lubrication change intervals are specific to the application and help ensure a smooth and healthy bearing operation [22]. According to SKF, the leading causes of bearing damage are lubrication (36%), contamination (23%), application (18%), interface (8%), handling (8%), electrical (5%) and fatigue (2%). A few studies have been conducted regarding the health of the wind turbine's main bearing. In [23], a novel prognostic approach to predict the remaining useful lifetime of bearings in a wind turbine's gearbox was proposed. The study relied on artificial neural networks to predict the short-term tendencies. The data-driven approach was specific to the bearings in the wind turbine gearbox. Another data-driven approach to analyse

bearing faults was discussed in [24], where data mining was applied to identify bearing faults in a wind turbine. The research relied on a neural network algorithm using the data collected from several wind turbines. The results from this study were the prediction of over-temperature events ahead of the fault occurrence. A study about the prediction and diagnosis of wind turbine faults is presented in [25]. The temperature parameters of SCADA data, such as bearing temperature, were used for fault detection. A long-term fault prediction framework was discussed in [26]. This study also utilised SCADA data and secondary measurements from 108 wind turbines with main-bearing failures. Historic wind turbine data for run-to-failure and non-run-to-failure wind turbines was utilized to predict the remaining power generation before failure in [27]. All these studies were data-based and focused on main-bearing-related issues such as the prediction of time-to-failure, over-temperature event prediction and remaining power generation before failure. However, there are no studies that use detailed wind turbine models to study the lifetime of the main bearing of the wind turbine. The impact of the provision of ancillary services on the health of the wind turbine's main bearing remains unknown. The main bearings of a wind turbine are subjected to dynamically varying forces during its operation. The forces are significantly more dynamic when providing ancillary services such as FCR. This originates from the control algorithms implemented to provide frequency control, which change the radial and axial forces acting upon the main bearing, hence affecting the overall health of the main bearing. A study of these forces and their impact on the lifetime of the main bearing of the wind turbine is important in times when wind turbines are expected to provide ancillary services. A study of the lifetime of the main bearing is also particularly relevant as it is a comparatively expensive component with a high replacement cost and a significant downtime for replacement. To this end, this study analyses and quantifies the effect of providing ancillary services on the lifetime and health of the wind turbine main bearing.

The article is organized as follows: Section 2 describes the models and data used for the study. These include the wind turbine, torque control, pitch control, main bearing, wind field design and data processing. In Section 3, the methodology used to calculate the forces acting on the wind turbine main bearing and the lifetime are explained. Section 4 presents and discusses the results from the simulated cases. The conclusions from the study are presented in Section 5.

2. Models and Data

The models used in this study include the wind turbine rotor, the permanent magnet synchronous generator, the control system and the main bearing. Additionally, wind data are used as an input for the simulations. These models and data are detailed in this section.

2.1. Wind Turbine

The wind turbine model used for this paper is a 5 MW reference wind turbine for offshore system development [28]. The wind turbine model uses broad design information from published documents of turbine manufacturers with a high correspondence with the REpower 5M machine. The model is developed in FAST v8, a high-fidelity wind turbine simulator developed by the National Renewable Energy Laboratory (NREL). The simulations are performed using the blade element momentum (BEM) option in the AeroDyn v15 module of FAST v8 [29]. Within AeroDyn there are four sub-models for rotor induction, blade airfoil aerodynamics, tower influence on the fluid local to the blade nodes and tower drag. The module calculates aerodynamic loads on the blades and the tower. The structural and aerodynamic properties of the blades are based on the 62.6 m long glass fibre blade used in the study presented in [30]. The structural model of the wind turbine is the Offshore Code Comparison Collaboration (OC3) monopile [31]. The main properties of this wind turbine are listed in Table 1.

The wind turbine of the defined type operates in three different regions. These regions, as presented in Figure 2, are based on the free-flow wind speed measured on the wind

turbine rotor. It can be seen in Figure 2 that Region 1 corresponds to wind speeds below 3 m/s, i.e., below the cut-in speed of the wind turbine. There is no torque generated in Region 1 and no power is extracted. In Region 2, the wind turbine operates in maximum power point tracking (MPPT) mode. In Region 3, the wind speeds are higher than the nominal wind speed. In this region, the torque, speed and power are limited using control methods in order to avoid overloading of the drivetrain components. In case the wind speed exceeds 25 m/s, the wind turbine is in the cut-out region and no power is produced.

Table 1. Wind turbine properties.

Property	Specification
Power rating	5 MW
Nominal torque	4 MN-m
Rotor orientation & configuration	Upwind, 3 blades
Rated rotor speed	12.1 rpm
Rotor and hub diameter	126 m and 3 m
Hub height	90 m
Cut-in, Rated and Cut-out wind speed	3 m/s, 11.4 m/s and 25 m/s

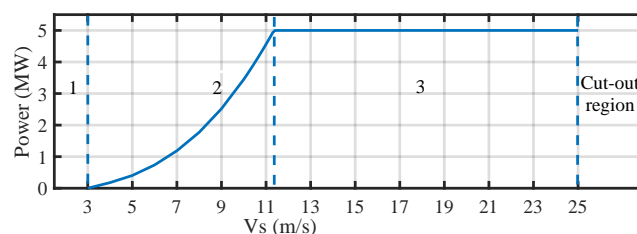


Figure 2. Power curve of a 5 MW wind turbine.

2.2. Main Bearing

The original wind turbine model developed by NREL does not consider the detailed features of the main bearing. However, since the wind turbine is largely based on the REpower 5M machine, the available literature and data about the bearing design and its properties were used. The schematic of the main bearing positioning in the wind turbine is shown in Figure 3. The bearing used in this machine is a spherical roller bearing, weighing 3320 kg [32].

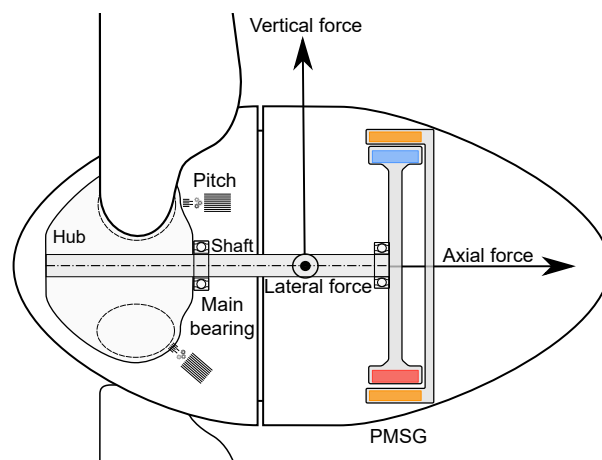


Figure 3. Main bearing position.

Since a detailed datasheet of the turbine's main bearing is not publicly available, some assumptions and estimates were made about the bearing's properties. The main property of the bearing that was required to calculate the lifetime is its basic dynamic load rating C

in Newtons, which represents the maximum load that a bearing can be subjected to for a rating life of one million revolutions. In order to estimate the C rating of the bearing, data from similar bearing types available through SKF were used in curve fitting. To double check, simulations were performed to calculate the load on the main bearing of the wind turbine to make sure that the load was always lower than the bearing rating.

2.3. Permanent Magnet Synchronous Generator

The generator used for this study was a permanent magnet synchronous generator (PMSG). The generator was modelled in a rotating direct, quadrature (d,q) reference frame. The generator parameters used in this model are listed in Table 2.

Table 2. Generator properties.

Property	Specification
Rated power	5 MW
Rated speed	12.1 rpm
Nominal efficiency	93%
Pole pairs	117
Nominal voltage	1950 V
Nominal current	876 A
Stator resistance	98.5 mΩ
Quadrature stator inductance	5.86 mH

2.4. Control

The different control schemes used in the study are detailed in this section.

2.4.1. Torque Control

A crucial part of this study is an effective torque control of the PMSG. To serve this purpose, field-oriented control (FOC) was used. In FOC, the quadrature current component (\hat{i}_q) was proportionally regulated to the torque setpoint. The direct current component (\hat{i}_d) was kept at zero to realize field orientation. The torque control scheme is presented in Figure 4. The proportional and integral gains of the proportional integral (PI) controller were set equal to 0.0001. At each time step, a current signal based on a comparison between the reference power (\hat{P}) and actual power (P) was generated by the controller. The reference power was based on the grid frequency and the amount of contracted ancillary reserve. The outputs of the PI controllers were then converted to three-phase abc signals using the inverse Park transformation. As a result, pulse width-modulated (PWM) signals corresponding to the three phases were generated. The PI controller was set up to minimize the tracking error by minimizing the overshoot and settling time. The performance of the developed controller varied with changing wind speed and the rate of change of the reference power. However, the controller was able to track the reference power with negligible error.

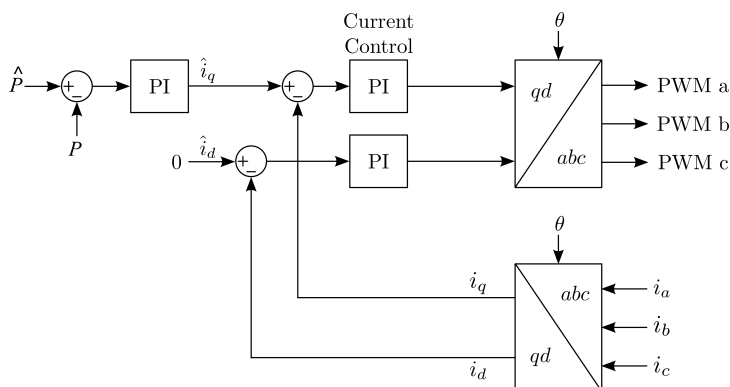


Figure 4. Field-oriented control.

The simulations were performed with four different cases. In the first case no FCR is provided, i.e., the wind turbine operates in the MPPT mode. In the second case, the wind turbine is de-loaded by 20%, i.e., the turbine operates at 80% of the maximum power curve. In the third and fourth cases 20 and 40% FCR is provided, i.e., 20 and 40% of the available power is reserved for FCR, respectively. For the 20% FCR case, the wind turbine control design is as shown in Figure 5. In Figures 5 and 6, the blue and red curves represent the upper and lower bound of the output power. The black curve represents the base power. The shaded area demonstrates the area of operation, i.e., the reference power at any given point lies within this area based on the grid frequency. The reference power for these cases was calculated by using Algorithm 1. The algorithm was designed such that a symmetrical 200 mHz frequency support is provided. A frequency response dead-band of 10 mHz centred at a nominal frequency (50 Hz) was present to reduce excessive control activities and turbine mechanical wear for normal power system frequency variations. Here, P_{UB} and P_{LB} are the upper and lower bound powers, respectively, as presented in Figures 5 and 6. The reference power P_{ref} was calculated as the sum of base power P_{base} and a time varying term $P_{freq}(t)$. $P_{freq}(t)$ was calculated using α which is proportional to the percentage of FCR provided, p_{FCR} . k is the proportionality constant with the value 0.25. α is defined as follows:

$$\alpha = k \cdot p_{FCR} \quad (1)$$

P_{base} is defined according to the black curve in Figures 5 and 6 for the 20 and 40% FCR cases, respectively. Furthermore, $P_{freq}(t)$ is based on the varying grid frequency f and the contracted FCR bid P_{FCR} , i.e., 20 or 40%.

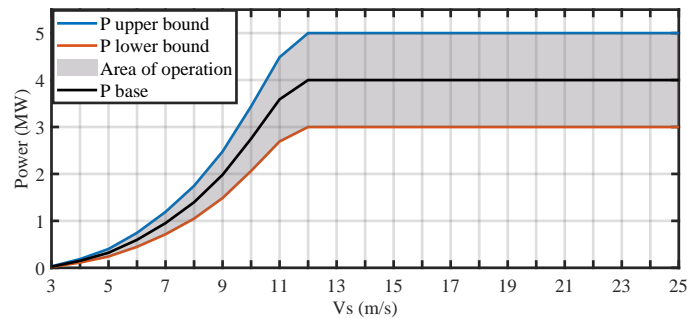


Figure 5. Control design for 20% FCR.

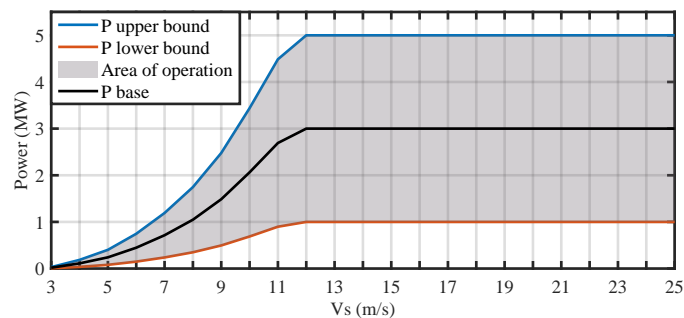


Figure 6. Control design for 40% FCR.

Algorithm 1 Reference power decision.

```

Require:  $P_{ref} \leq P_{UB}$ 
if  $f \leq 49.8$  Hz then
     $P_{ref}(t) = P_{UB}$ 
else if  $49.80$  Hz  $< f < 49.99$  Hz then
     $P_{ref}(t) = P_{base} + P_{freq}$  ▷  $P_{freq}=\alpha(50-f)$ 
else if  $49.99$  Hz  $< f < 50.01$  Hz then
     $P_{ref}(t) = P_{base}$  ▷ 10 mHz deadband
else if  $50.01$  Hz  $< f < 50.20$  Hz then
     $P_{ref}(t) = P_{base} + P_{freq}$  ▷  $P_{freq}=\alpha(50-f)$ 
else if  $f \geq 50.20$  Hz then
     $P_{ref}(t) = P_{LB}$ 
end if ▷ all powers given in MW
    
```

2.4.2. Pitch Control

The pitch control system developed in Simulink was connected to the wind turbine model in FAST. On every loop of the simulation, the pitch control system sends a pitch command to the wind turbine for each of the three blades. The block diagram of the pitch control system is presented in Figure 7. The pitch control is a PI controller with proportional and integral gains equal to 206.3 and 25, respectively. The reference rotor speed Ω_{ref} is a set parameter to which the actual rotor speed Ω is compared at each time step by the PI controller. The gain scheduling is implemented by a dimensionless gain correction factor G as defined below. Here, θ is the pitch angle and θ_d is a tuning parameter set at 0.055 radians [33].

$$G = \frac{1.6}{1 + \left(\frac{\theta}{2\theta_d}\right)} \tag{2}$$

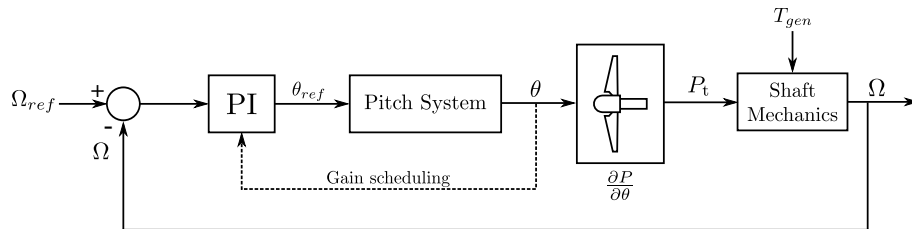


Figure 7. Pitch control of the wind turbine blades.

2.5. Wind Field Design and Data Processing

The wind data used for the simulations in this research work are from the publicly available data repository of meteorological data provided by Ørsted. The data are available for several offshore meteorological stations [34]. The LiDAR data are 10 min statistics for wind measurements from LiDARs installed at offshore wind farms. A total of 2 years of data sampled at 10 min were used. In order to fit the data to the operating range of the wind turbine, the data were processed to fit the requirements. Firstly, only the data within the range of wind velocities between 3 and 25 m/s were retained. The wind data were then rounded off to the nearest integer. These data can be visualised in graphical form as presented in Figure 8. Figure 8 shows the probability of occurrence of different levels of wind speed within the operating range of the wind turbine. The simulations were performed for each of these wind levels, and their probability of occurrences was used to deduce the final results.

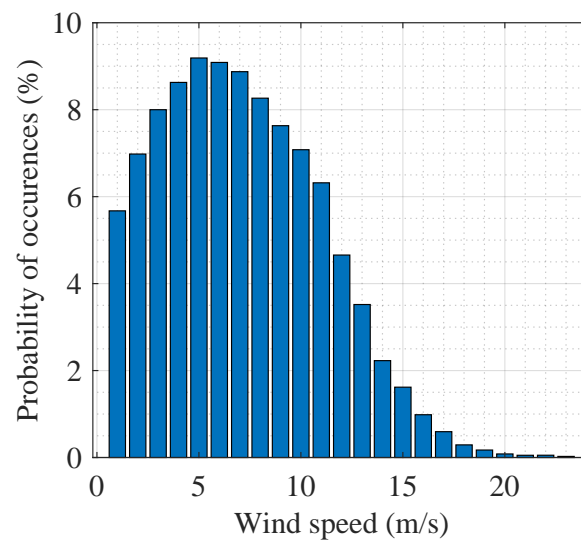


Figure 8. Wind speed percentage occurrences.

3. Methodology

Different outputs from these simulations were analysed and used for the calculation of bearing loads and lifetime. These parameters are presented in the following subsections.

3.1. Dynamic Equivalent Force

There are different forces acting on the blade root of the wind turbine and hence the main bearing. The axial, vertical and lateral forces are shown in Figure 3. These forces were used to calculate the dynamic equivalent force. The axial force was measured at the root of each blade. The three individual blade forces were then averaged, as shown in (3). Here, F_{b1} , F_{b2} and F_{b3} represent the axial forces, F_a (in Newtons) at the three blades of the wind turbine.

The radial force, on the other hand, was given as a result of the lateral force F_l and the vertical force F_v acting on the blade root, as shown in Figure 3. The equation is given in Equation (4).

$$F_a = \frac{F_{b1} + F_{b2} + F_{b3}}{3} \quad (3)$$

$$F_r = \sqrt{F_l^2 + F_v^2} \quad (4)$$

The dynamic equivalent force P_d in Newtons is defined in Equation (5), where b_x and b_y are the dimensionless empirical factors for the specific spherical roller bearing. The SKF catalogue for rolling bearings [35] suggests that the mean force, F_m (in Newtons) should be calculated considering their minimum and maximum values. Therefore, the mean values of radial and axial forces were calculated using Equation (6), where F_{\min} and F_{\max} represent the minimum and maximum values of the forces within the steady period of the entire simulation time.

$$P_d = b_x F_r + b_y F_a \quad (5)$$

$$F_m = \frac{F_{\min} + 2F_{\max}}{3} \quad (6)$$

3.2. Lifetime

The linear fatigue damage accumulation method used in this study was based on [36]. The method incorporates the weight and dynamic equivalent force of each load level. Hence, providing a good estimate for the bearing lifetime. In this method, firstly L_i is defined as the number of revolutions spent at a given wind speed by the main bearing. L_i

is calculated as in Equation (7). Here, t_i is the number of hours of load level i . Ω is the speed in *rpm* for load level i .

$$L_i = t_i \Omega_i 60 \quad (7)$$

Next, the basic rating life L_{10_i} is defined as the life required for 10 % of bearing samples to fail, for an identical group of bearings at a given load level i . L_{10_i} was calculated as given in Equation (8). Here, p is a bearing specific value, which is equal to 10/3 for roller bearings as per SKF.

$$L_{10_i} = 10^6 \left(\frac{C}{P_d} \right)^p \quad (8)$$

Thereafter, f_i is a fraction of the level i , defined to assign weight to individual load levels (1 to m). f_i was calculated as in Equation (9).

$$f_i = \frac{L_i}{\sum_{i=1}^m L_i} \quad (9)$$

The combined lifetime (in years) including all load levels was determined by Equation (10). Here, a_1 , a_2 and a_3 represent the life modification factors. a_1 was set equal to 0.21 corresponding to a 99% reliability of the main bearing surviving the estimated lifetime. The factors a_2 and a_3 correspond to the material of the bearing and lubrication conditions and these were set equal to 1.

$$L_M = \frac{1}{\sum_{i=1}^m \left(\frac{f_i}{L_{10_i}} \right)} \frac{a_1 a_2 a_3}{10^6} \quad (10)$$

4. Results and Discussion

For this study, four different cases were designed. For each case, 23 simulations were performed. These 23 simulations were designed such that for each integer wind speed within the operating range (3–25 m/s) of the wind turbine, a simulation was conducted. In this manner, the entire operating range of the wind turbine was included in the study. The main outputs from these simulations, namely axial, radial and dynamic equivalent forces were then used to calculate the lifetime of the main bearing of the wind turbine. These simulations considered the forces once the wind turbine had reached a steady operation.

These four cases differed from each other in the type of control applied. Case 1 is where the wind turbine operates to provide maximum available power. Therefore, no margin in the active power is retained to provide an FCR service. The wind turbine operates on either MPPT or power-limiting control, based on the wind speed. In Case 2, the control is such that the reference power is de-loaded by 20%. Apart from de-loading, the operation of the wind turbine remains similar to Case 1, and no FCR is provided. Figure 9 presents the reference power for curves for Case 1 and Case 2. The blue curve presents Case 1 and the red presents Case 2. It can be seen here that for each individual wind speed load level, a different reference power is set for the two cases.

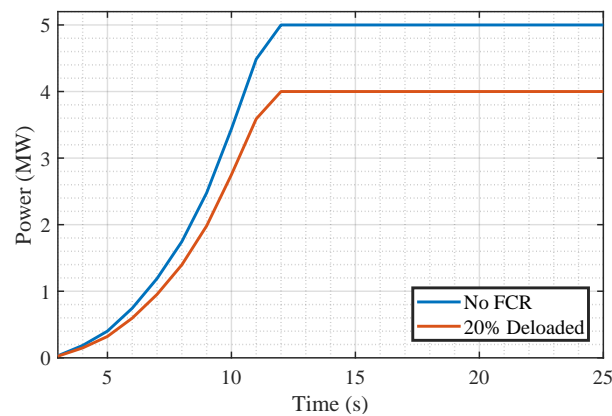


Figure 9. Power reference for the no FCR and 20% de-loaded cases.

Case 3 and Case 4 were comparative cases that were simulated to observe the effect of providing FCR on the main bearing of the wind turbine. In these cases the wind turbine control systems based on Algorithm 1 were used. Figure 10 consists of three different curves. The red curve corresponding to the right y -axis represents the grid frequency. The first blue curve on the top, corresponding to the left y -axis represents Case 3 where the wind turbine provides 20% FCR. The second blue curve at the bottom represents Case 4 where the wind turbine provides 40% FCR. As can be observed from Figure 10, the reference power changes to accommodate the real-time changes in FCR requirements based on the grid frequency.

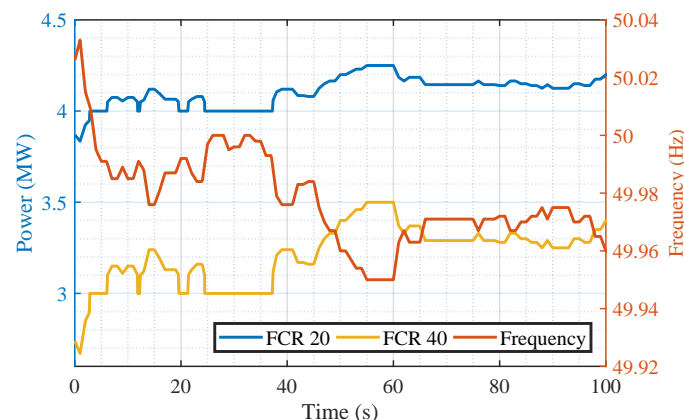


Figure 10. Power reference for the 20 and 40% FCR cases.

Figure 11 presents nine different graphs to present the dynamic axial, radial and equivalent forces acting on the main bearing. The load levels presented in Figure 11 correspond to the wind speeds of 4, 12 and 25 m/s. These levels were chosen such that the forces in low-, medium- and high-wind speed ranges can be presented. However, it should be noted that the simulations were performed for each load level from 3 to 25 m/s.

In Figure 11, each graph consists of four curves, representing the four cases, i.e., no FCR, 20% de-loaded, 20% FCR, and 40% FCR. Figure 11a–c present the axial forces for the three load levels. It can be seen that the first two curves, corresponding to no FCR and 20% de-loaded, even though oscillating ($V_s = 12$ and 25 m/s, respectively), are relatively steady compared to the last two curves, where FCR is provided. Considering the varying grid frequency, the power output is changed through torque and pitch control, resulting in a varying axial force.

Figure 11d–f present the radial forces for the three load levels. The radial forces for each of these cases is relatively lower compared to the axial forces. For the low-wind speed of 4 m/s, in Figure 11d, the radial forces are close for these cases. Providing FCR exhibits a clear effect on the radial forces, as seen in Figure 11e.

Figure 11g–i present the dynamic equivalent force. The dynamic equivalent force was calculated as explained in Section 3.1. The combined effect of both axial and radial forces can be observed here. The impact of these two forces on the calculated P_d is dependent on the empirical factors b_x and b_y . The lifetime of the main bearing of the wind turbine is directly related to its basic dynamic load rating C . The value of C varies based on the strength of the bearing. In order to study the loading and lifetime depending on different design choices, the range of $0.75C$ to $1.25C$ was used in the simulations, where C was as defined in Section 2.2.

The results of bearing lifetime are presented in Table 3. The results show that the highest lifetime was observed in the case with no FCR for all C values. It can be seen that the difference in lifetime compared to the other three cases is higher for higher C values and lower for lower C values. It can also be seen that the values for the 20% de-loaded and 20% FCR cases are close. The least lifetime was observed for the 40% FCR case. The results here firstly point to the effect of a higher C rating on the bearing lifetime. A higher C value consistently gave a higher lifetime estimate for the main bearing. Secondly, a lifetime reduction for the main bearing is associated with providing FCR. Figure 12 presents a graph of the change in lifetime with increasing α , where α represents the amount of provided FCR. The different curves in Figure 12 represent the lifetime for different C ratings corresponding to the basic dynamic load rating values. It is seen that the main bearing lifetime reduces with increasing α . However, for the higher C rating cases, the lifetime is higher than the average lifetime of the studied wind turbine, i.e., 20 years. An informed decision can be made based on this research and the economics of wind turbine operation, such that if the cost of using a high C -rated main bearing can be compensated for by the revenue generated from the provision of FCR, then it is indeed an advantage to provide FCR with a wind turbine. On the other hand, if the C rating of the main bearing is low, it is not advisable to provide FCR due to its detrimental impact on lifetime.

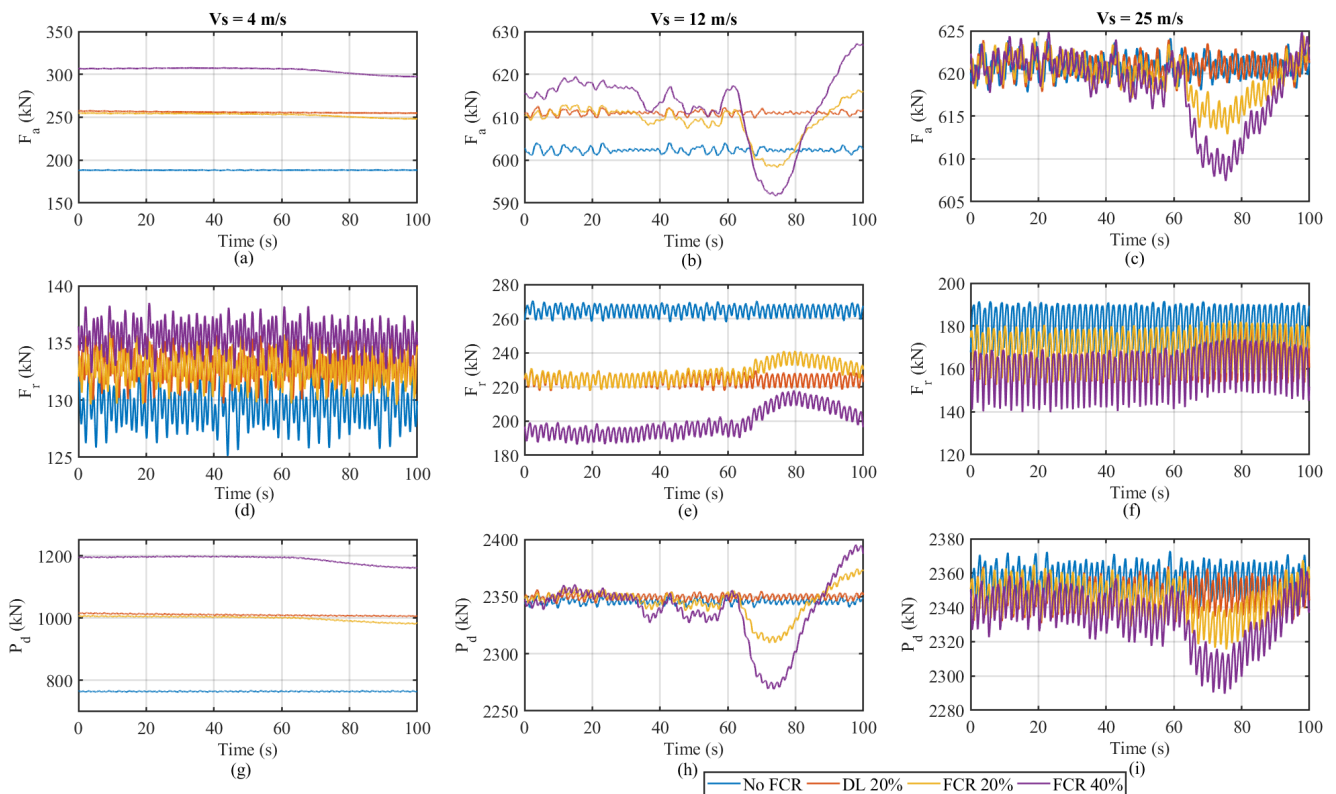


Figure 11. Dynamic forces acting on the wind turbine's main bearing.

Table 3. Bearing life, in years.

C	No FCR	20% deloaded	20% FCR	40% FCR
0.75	13.88	8.88	9.02	8.1
0.8	17.21	11.01	11.19	10.02
0.85	21.06	13.48	13.7	12.26
0.9	25.49	16.31	16.57	14.84
0.95	30.52	19.53	19.84	17.77
1	36.21	23.17	23.54	21.08
1.05	42.6	27.27	27.7	24.81
1.1	49.75	31.84	32.35	28.97
1.15	57.69	36.92	37.51	33.6
1.2	66.49	42.55	43.23	38.71
1.25	76.18	48.75	49.53	44.36

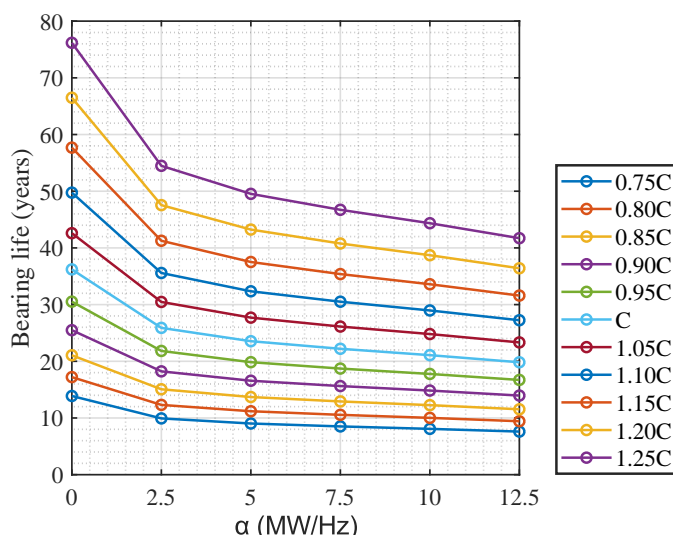


Figure 12. Bearing life vs. α for the different basic dynamic load rating values.

5. Conclusions

In this paper, the bearing lifetime of a wind turbine primary shaft was studied. The importance of this study lies in the fact that there is an increasing participation of wind turbines in the ancillary services market. This participation is expected to grow in the coming years as a result of the higher penetration of wind power in the energy grid. In such a scenario, it is crucial to conduct research on the impact of providing ancillary services on wind turbine components. The scope of this study focussed on a specific component of the wind turbine, its main bearing. The choice of this component was based on the relative cost and downtime associated with the maintenance and replacement of this component. The study explored several different cases and methods of FCR control. A common observation from this study was the clear impact of providing FCR on the lifetime of a wind turbine’s main bearing. The study concludes that the impact of FCR provision on the lifetime of the main bearing is subjective to the amount of FCR provided and its C rating. Considering the base case with no FCR provision, a lifetime reduction of 36% was observed for the case when the wind turbine was operated with 20% de-loaded. A lifetime reduction of 35 and 41.8% was observed for the cases of 20 and 40% FCR, respectively. This trend holds for the entire range of C ratings simulated in this study. It was also observed that to achieve the same bearing lifetime as the case with no FCR provision, an oversizing of approximately 15 and 20% in the C rating was required for the 20 and 40% FCR cases, respectively. Based on this study a higher FCR provision is suggested for a wind turbine consisting of bearings with a higher basic dynamic load rating.

Author Contributions: Conceptualization, N.S., J.D.M.D.K. and L.V.; methodology, N.S. and D.B.; software, N.S.; validation, N.S.; formal analysis, N.S.; writing—original draft preparation, N.S.; writing—review and editing, N.S., J.D.M.D.K. and L.V.; visualization, N.S., J.D.M.D.K. and L.V.; supervision, J.D.M.D.K., W.D.W. and L.V.; funding acquisition, L.V. and J.D.M.D.K. All authors have read and agreed to the published version of the manuscript.

Funding: This research was conducted in the frame of the BEOWIND project, funded by the Energy Transition Fund of the Belgian Federal Government.

Data Availability Statement: The data used in the current study are available from the corresponding author upon reasonable request.

Conflicts of Interest: The authors declare no conflict of interest.

References

1. Global Wind Energy Council. Global Wind Report. 2022. Available online: <https://gwec.net/global-wind-report-2022/> (accessed on 1 September 2022).
2. IRENA. *Renewable Energy Statistics 2022*; The International Renewable Energy Agency: Abu Dhabi, United Arab Emirates, 2022. Available online: <https://www.irena.org/> (accessed on 1 September 2022).
3. Energy Roadmap 2050 Energy. 2012. Available online: <https://ec.europa.eu/energy/> (accessed on 1 September 2022).
4. Wind Energy in Europe. Available online: <https://proceedings.windeurope.org/> (accessed on 1 September 2022).
5. Technical Requirements for the Connection of Generating Stations to the Hydro-Québec Transmission System. 2019. Available online: <http://www.hydroquebec.com/> (accessed on 1 September 2022).
6. European Association for Storage of Energy. Ancillary Services. 2021. Available online: <https://ease-storage.eu/wp-content/uploads/2021/08/Ancillary-Services.pdf> (accessed on 6 May 2022).
7. Hughes, G. *The Performance of Wind Farms in the United Kingdom and Denmark*; Renewable Energy Foundation: London, UK, 2012. Available online: <http://tinyurl.com/cn5qnqg> (accessed on 1 September 2022).
8. Ribrant, J.; Bertling, L. Survey of Failures in Wind Power Systems With Focus on Swedish Wind Power Plants During 1997–2005. *IEEE Trans. Energy Convers.* **2007**, *22*, 167–173. [\[CrossRef\]](#)
9. Tavner, P.; Xiang, J.; Spinato, F. Reliability analysis for wind turbines. *Wind Energy* **2007**, *10*, 1–18. [\[CrossRef\]](#)
10. Arwade, S.; Lackner, M.; Grigoriu, M. Probabilistic Models for Wind Turbine and Wind Farm Performance. *J. Sol. Energy Eng.* **2011**, *133*, 041006. [\[CrossRef\]](#)
11. Conroy, N.; Deane, J.; Gallachóir, B.Ó. Wind turbine availability: Should it be time or energy based?—A case study in Ireland. *Renew. Energy* **2011**, *36*, 2967–2971. [\[CrossRef\]](#)
12. Staffell, I.; Green, R. How does wind farm performance decline with age? *Renew. Energy* **2014**, *66*, 775–786. [\[CrossRef\]](#)
13. Managing the wind: Reducing kilowatt-hour costs with condition monitoring. *Refocus* **2005**, *6*, 48–51. [\[CrossRef\]](#)
14. Deutsch, J.; He, D. Using Deep Learning-Based Approach to Predict Remaining Useful Life of Rotating Components. *IEEE Trans. Syst. Man Cybern. Syst.* **2018**, *48*, 11–20. [\[CrossRef\]](#)
15. Yang, W.; Tavner, P.J.; Crabtree, C.J.; Wilkinson, M. Cost-Effective Condition Monitoring for Wind Turbines. *IEEE Trans. Ind. Electron.* **2010**, *57*, 263–271. [\[CrossRef\]](#)
16. Pedregal, D.; García, F.; Roberts, C. An algorithmic approach for maintenance management based on advanced state space systems and harmonic regressions. *Ann. Oper. Res.* **2008**, *166*, 109–124. [\[CrossRef\]](#)
17. Raouf, A. Maintenance Excellence: Optimizing Equipment Lifecycle Decision. *J. Qual. Maint. Eng.* **2004**, *10*, 75. [\[CrossRef\]](#)
18. Marquez, F.P.G. An Approach to Remote Condition Monitoring Systems Management. In Proceedings of the 2006 IET International Conference on Railway Condition Monitoring, Birmingham, UK, 29–30 November 2006; pp. 156–160.
19. García, F.P.; Pedregal, D.J.; Roberts, C. Time series methods applied to failure prediction and detection. *Reliab. Eng. Syst. Saf.* **2010**, *95*, 698–703. [\[CrossRef\]](#)
20. Byon, E.; Ding, Y. Season-Dependent Condition-Based Maintenance for a Wind Turbine Using a Partially Observed Markov Decision Process. *IEEE Trans. Power Syst.* **2010**, *25*, 1823–1834. [\[CrossRef\]](#)
21. Yeghikian, M.; Ahmadi, A.; Dashti, R.; Esmailion, F.; Mahmoudan, A.; Hoseinzadeh, S.; Garcia, D.A. Wind Farm Layout Optimization with Different Hub Heights in Manjil Wind Farm Using Particle Swarm Optimization. *Appl. Sci.* **2021**, *11*, 9746. [\[CrossRef\]](#)
22. Bearing Damage and Failure Analysis. Report. Available online: <https://www.skf.com> (accessed on 3 March 2023).
23. Teng, W.; Zhang, X.; Liu, Y.; Kusiak, A.; Ma, Z. Prognosis of the Remaining Useful Life of Bearings in a Wind Turbine Gearbox. *Energies* **2017**, *10*, 32. [\[CrossRef\]](#)
24. Kusiak, A.; Verma, A. Analyzing bearing faults in wind turbines: A data-mining approach. *Renew. Energy* **2012**, *48*, 110–116. [\[CrossRef\]](#)
25. Kusiak, A.; Li, W. The prediction and diagnosis of wind turbine faults. *Renew. Energy* **2011**, *36*, 16–23. [\[CrossRef\]](#)
26. Herp, J.; Pedersen, N.; Nadimi, E. A Novel Probabilistic Long-Term Fault Prediction Framework Beyond SCADA Data—With Applications in Main Bearing Failure. *J. Phys. Conf. Ser.* **2019**, *1222*, 012043. [\[CrossRef\]](#)

27. Wiese, B.; Pedersen, N.; Nadimi, E.; Herp, J. Estimating the Remaining Power Generation of Wind Turbines—An Exploratory Study for Main Bearing Failures. *Energies* **2020**, *13*, 3406. [[CrossRef](#)]
28. Jonkman, J.; Butterfield, S.; Musial, W.; Scott, G. Definition of a 5-MW Reference Wind Turbine for Offshore System Development. 2009. Available online: <https://www.nrel.gov/docs/fy09osti/38060.pdf> (accessed on 1 September 2022).
29. Jonkman, J.M.; Hayman, G.J.; Jonkman, B.J.; Damiani, R.R.; Murray, R.E. AeroDyn v15 User's Guide and Theory Manual, NREL. Available online: <https://www.nrel.gov/wind/nwtc/assets/pdfs/aerodyn-manual.pdf> (accessed on 1 September 2022).
30. Lindenburg, C. *Aeroelastic Modelling of the LMH64-5 Blade*; DOWEC Dutch Offshore Wind Energy Converter 1997–2003 Public Reports; Energy Research Center of The Netherlands: Petten, The Netherlands, 2002.
31. Jonkman, J.; Butterfield, S.; Passon, P.; Larsen, T.; Camp, T.; Nichols, J.; Azcona, J.; Martinez, A. Offshore Code Comparison Collaboration within IEA Wind Annex XXIII: Phase II Results Regarding Monopile Foundation Modeling. In Proceedings of the 2007 European Offshore Wind Conference & Exhibition, Berlin, Germany, 4–6 December 2007.
32. The Great Power. 2005. Available online: <https://evolution.skf.com/the-great-power-3/> (accessed on 1 September 2022).
33. Samani, A.; De Kooning, J.; Kayedpour, N.; Singh, N.; Vandeveld, L. The Impact of Pitch-To-Stall and Pitch-To-Feather Control on the Structural Loads and the Pitch Mechanism of a Wind Turbine. *Energies* **2020**, *13*, 4503. [[CrossRef](#)]
34. Offshore Wind Data. Orsted.com. 2022. Available online: <https://orsted.com/en/our-business/offshore-wind/wind-data> (accessed on 1 September 2022).
35. SKF. Rolling Bearings. 2018. Available online: <https://www.skf.com/group/products/rolling-bearings> (accessed on 1 September 2022).
36. Zaretsky, E. A. *Palmgren Revisited: A Basis For Bearing Life Prediction*; National Aeronautics and Space Administration: Washington, DC, USA, 1997.

Disclaimer/Publisher's Note: The statements, opinions and data contained in all publications are solely those of the individual author(s) and contributor(s) and not of MDPI and/or the editor(s). MDPI and/or the editor(s) disclaim responsibility for any injury to people or property resulting from any ideas, methods, instructions or products referred to in the content.